Shear-induced structuring of phase-separated sodium caseinate - sodium alginate blends using extrusion-based 3D printing: Creation of anisotropic aligned micron-size fibrous structures and macroscale filament bundles

Sicong Zhu [a], Wenwei Wang [a], Markus Stieger [b], Atze Jan van der Goot [a], Maarten A. I. Schutyser [a,*]

[a] *Laboratory of Food Process Engineering, Wageningen University, Bornse Weilanden 9, 6708WG Wageningen, the Netherlands*
[b] *Division of Human Nutrition and Health and Food Quality and Design, Wageningen University, Stippeneng 4, 6708WE Wageningen, the Netherlands*

ABSTRACT

3D food printing is considered a promising method to prepare personalized foods having unique macroscopic design and composition. It is still challenging to create 3D printed foods with tailored microstructure, e.g. fibrous microstructures, to print meat-like foods. In this study we investigated the preparation of 3D printed model food gels that have macro- and microscale aligned fibrous structures using sodium caseinate - sodium alginate (SC/SA) blends with extrusion-based printing. A bath containing an agar fluid gel was used to allow precise deposition and solidification of the SC/SA blend after the printing process. Besides, the influences of nozzle type and printing speeds on texture were assessed. We succesfully created aligned micron-size fibrous structures and macroscale aligned filament bundles. Filaments extruded using tapered nozzles had finer fibrous structures compared to those extruded using straight nozzles. Both printing speed and nozzle type significantly influenced Young's moduli of 3D printed model food gels. A higher printing speed resulted in smaller Young's moduli of individual printed filaments. This study shows that anisotropic structures can be created by extrusion-based 3D printing of phase-separated sodium caseinate - sodium alginate blends. The results of this study might become relevant when striving for meat analogues made by 3D-printing.

1. Introduction

Driven by health awareness and environmental concerns among consumers, the global market of meat analogues shows rapid growth in recent years (Ismail, Hwang, & Joo, 2020). Various food manufacturing technologies such as extrusion cooking and shear cell technology have been studied to create whole cut types of meat analogues that display both microscale and macroscale anisotropic fibrous structures (Kyriakopoulou, Dekkers, & van der Goot, 2018). The underlying texturizing mechanism is known as the solidification of phase-separated food systems in which a liquid dispersed phase is deformed and aligned under shear flow (Dekkers, Boom, & van der Goot, 2018; Tolstoguzov, 2006). Dekkers, Nikiforidis, and van der Goot (2016) obtained fibrous structures with a blend of pectin and soy protein isolate using shear cell technology. The authors observed that elongated pectin filaments being oriented in the direction of shear flow were entrapped in a continuous soy protein phase. In both extrusion cooking and shear cell technology, the solidification process of phase-separated systems was achieved through cooling, where the continuous, soy protein rich phase transits from a viscous state to a more elastic state (Pietsch, Bühler, Karbstein, & Emin, 2019; Schreuders et al., 2021). Shear-induced structuring of phase-separated food blends can also be achieved using other technologies that generate desired shear flow. Examples of those technologies include microfluidic devices (Takayama & Kato, 2018), spinning and extrusion-based 3D printers.

Extrusion-based 3D printing is an emerging food manufacturing technique that allows layer by layer deposition of three-dimensional structures according to a digital design (Sun, Zhou, Huang, Fuh, & Hong, 2015). 3D printing has the potential to create foods with complex shapes (BluRhapsody, 2022), personalized nutrition (Escalante-Aburto, Trujillo-de Santiago, Álvarez, & Chuck-Hernández, 2021) and to alter sensory perception of foods (Khemacheevakul, Wolodko, Nguyen, & Wismer, 2021; Kistler, Pridal, Bourcet, & Denkel, 2021; Zhu et al., 2021). To date, only few studies have investigated the creation of

aligned fibrous structures that might be considered meat-like structures using 3D printing technologies (Kim, Kim, & Park, 2021; Ko et al., 2021). In these studies the 3D printed aligned fibrous structures had mostly a diameter around 1 mm, which is much larger than that of real muscle fibres (20–100 μm) (Feher, 2017). In order to create 3D printed micro-scale fibrous structures, new printing formulations and adapted printing methods are required. A promising approach is the use of protein-polysaccharide blends, e.g. caseinate-alginate mixtures that were recently employed to create micron size fibril bundles (Takayama & Kato, 2018). Caseinate-alginate mixture were extruded with a co-flow microfluidic device during which fibrous micro-structures were formed. Subsequently, the structures were solidified in calcium chloride solutions. The influence of the shear profile during the extrusion process on micro fibrillar structure formation is unknown. Additionally, it is not known whether or how the extruded fibres can be bundled into larger macroscopic structures.

3D printing of viscous liquids, i.e. caseinate-alginate mixtures, can be challenging since the extruded viscous liquids do not hold their shape after deposition onto a platform. 3D printing of caseinate-alginate mixtures into calcium-containing solutions is also not possible because the printed filaments are easily dragged by the moving print head, which causes printing failure. Recently, a 3D bioprinting technique termed "Freeform Reversible Embedding of Suspended Hydrogels (FRESH) has been developed to enable deposition of hydrogels (Hinton et al., 2015). The FRESH technique applies a supporting bath consisting of thermo-reversible gelatine microparticles that can initiate gelling of printed bio-ink due to the presence of crosslinking compounds. Such gel systems are often referred to as fluid gels, i.e. a suspension of gelled particles that are dispersed in a non-gelled continuous medium (Garrec & Norton, 2012). The advantage of fluid gels is that they behave as a fluid when sheared but as a solid in rest.

In this study we investigated the use of extrusion-based 3D printing to prepare fibre bundles using caseinate-alginate blends and create macroscale fibrous structures via layer-by-layer deposition. We investigated the influence of extrusion conditions on the microstructural change of caseinate-alginate (SC/SA) blends and the feasibility of creating both macroscale and microscale aligned fibrous structures using extrusion-based 3D printing technology. First, SC/SA blends were prepared and extruded with different extrusion speeds and nozzle types, and the obtained structures and textures were assessed by microscopic and tensile mechanical analysis. To enable accurate deposition and solidification of the extruded SC/SA fibre bundles, the extrudate was deposited into an agar fluid gel bath. Finally, the solidification process and textural properties of the structures were studied to identify the conditions required to obtain macroscopic anisotropic fibrous structures.

2. Materials and methods

2.1. Materials

A concentrated sodium caseinate dispersion (48% dry matter content) was kindly provided by Royal FrieslandCampina. Sodium alginate powder (Rudin®ProVega, Netherlands) was kindly provided by Ruitenberg Ingredients. Calcium chloride ($CaCl_2$) (Sigma-Aldrich, Netherlands) and Agar powder (Sigma-Aldrich, Netherlands) were purchased from MilliporeSigma.

2.2. Preparation of SC/SA blend

SC/SA blends were prepared according to (Capron, Costeux, & Djabourov, 2001; Takayama & Kato, 2018) with slight modifications. A 10 wt% sodium caseinate dispersion was prepared by mixing concentrated sodium caseinate with Milli-Q water and stirred at 80 °C for 30 min. The 10 wt% sodium caseinate dispersion was centrifuged at 15000*g* at 20 °C for 60 min to remove any undissolved aggregates. A 4 wt% sodium

alginate solution was prepared by mixing sodium alginate powder with Milli-Q water. The sodium alginate solution was stirred at 80 °C for 30 min followed by additional stirring at room temperature for 30 min to ensure dissolution of sodium alginate. A mixture of sodium caseinate and sodium alginate (SC-SA stock solution) was prepared by mixing 660 g of 10 wt% sodium caseinate dispersion with 220 g of 4 wt% sodium alginate solution and stirring at room temperature for 60 min. The SC-SA stock solution was centrifuged at 15000 G at 20 °C for 2 h to separate the alginate-rich phase (top) from the caseinate-rich phase (bottom). The SC/SA blend was obtained by mixing 30 g SC-rich phase with 70 g SA-rich phase at 300 rpm for 2 min using a planetary mixer (Thinky ARV 310, Japan). An overview of the preparation procedures for the SC-SA stock solution, SA-rich phase, SC-rich phase and SC/SA blend is shown in Fig. 1.

2.3. Preparation of agar fluid gels

A 1 wt% agar solution (aq) was heated at 90 °C for 30 min to allow dissolution. To obtain agar fluid gels, the heated agar solution was passed through a lab-scale colloid mill (IKA magic LAB®, IKA Staufen, Germany) with circulating cooling water of 5 °C. The gap width was set to 0.159 mm and a rotational speed of 20,000 rpm was applied. The shearing-cooling process was repeated until the agar fluid gel reached a temperature of 15 °C. $CaCl_2$ was added to agar fluid gel in order to crosslink printed SC/SA blend. To study the influence of $CaCl_2$ on the rheological properties of the agar fluid gel, $CaCl_2$ was either added to a heated agar solution before the shear-cooling process or directly mixed into the obtained agar fluid gel. $CaCl_2$ was added to heated agar solution or already prepared agar fluid gel at various concentrations (0.12, 0.25, 0.33, 0.55 and 1.1 wt%).

2.4. Rheology characterization of the agar fluid gel

Rheological measurements were carried out with a MCR 502 rheometer (Anton Paar, Austria) equipped with a concentric cylinder (CC17). A Step test with pre-set oscillation for three test intervals was used to assess the breakdown of the agar fluid gel under shear and its subsequent recovery. A pre-set shear strain (1%) was applied for the first and third test intervals to simulate the behaviour at rest before and after high shearing. For the second test interval, the strain was set to 100% to simulate the flow behaviour when moving the printing nozzles inside a fluid gel. Measurements were performed for 30 s each for the first and second test interval, and 120 s for the thirst test interval. All measurements were done at 20 °C using a frequency of 1 Hz. The storage modulus (G') at the end of the first interval was obtained, and structural regeneration was determined as the percentage of recovery of G' at 60 s in the third interval compared with the G' at the end of first interval.

2.5. Single filament extrusion of SC/SA blends

To study the influence of shear profiles on microstructure of SC/SA blends during the extrusion process, SC/SA blends were loaded into a 30 mL syringe barrel and extruded into a 0.12 wt% $CaCl_2$ solution using a Harvard PHD 4400 syringe pump (Harvard apparatus, USA). Four nozzle tips with an outlet diameter of 0.84 mm were used for extrusion, among which three straight tips (Optimum® general purpose dispense tips, Nordson EFD) that varied in length (6.35, 25.4, and 38.1 mm) and had a tapered tip (Optimum® SmoothFlow™ tapered dispensing tips, Nordson EFD) (31.2 mm) (See Fig. 2). The SC/SA blends were extruded at 3 different volumetric flow rates (19.94, 49.85, and 99.20 mL/h) which was achieved by applying three different printing speeds (10, 25, 50 mm/s) during the 3D printing process. The extruded filaments were kept in $CaCl_2$ solution for 30 min and then heated in a water bath for 10 min at 90 °C. Subsequently, filaments were washed with Milli Q water to remove excess $CaCl_2$ and stored for further analysis.
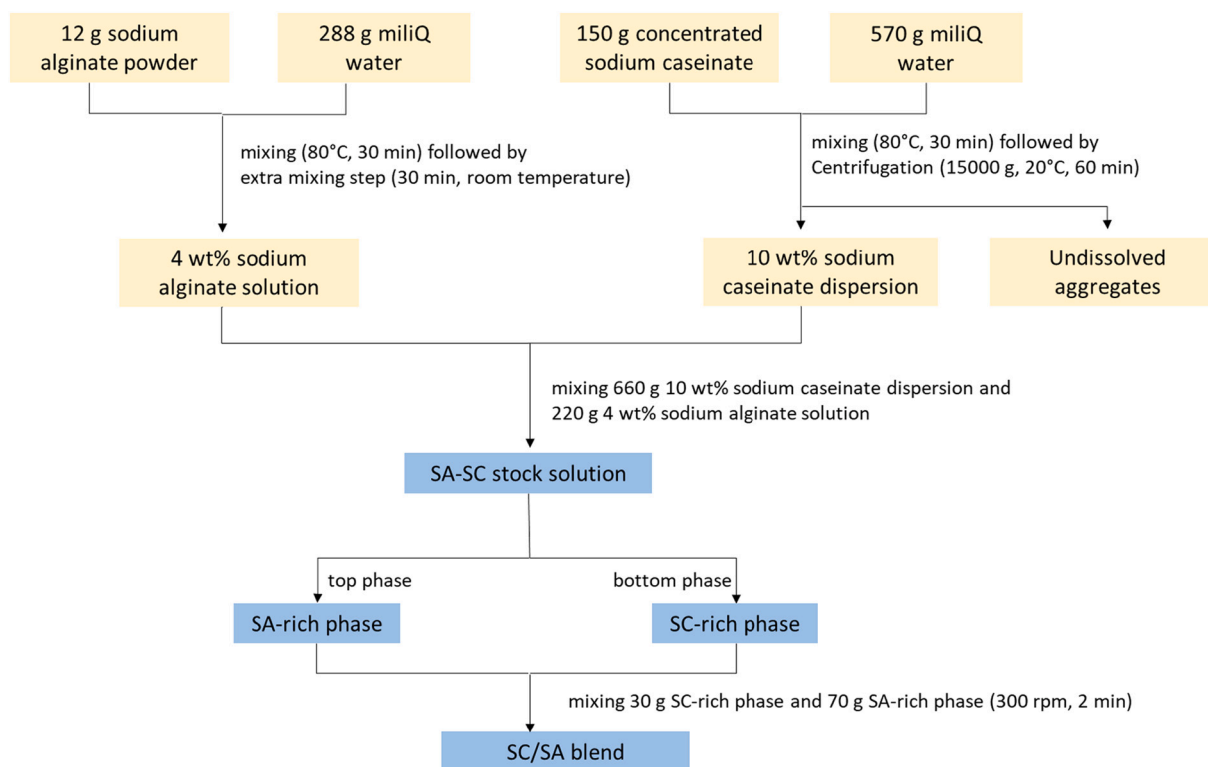
Fig. 1. Overview of the preparation procedures for the SC-SA stock solution, SA-rich phase, SC-rich phase and SC/SA blend.

Fig. 2. Nozzle tips used for extrusion and printing. Nozzles from left to right: long straight nozzle (metal part 38.1 mm), medium straight nozzle (metal part 25.4 mm), short straight nozzle (metal part 6.35 mm) and tapered nozzle (31.2 mm). All nozzles have outlet diameter of 0.84 mm.

2.6. 3D printing of the SC/SA blend

Printing experiments were performed using a byFlow 3D printer (byFlow B.V., the Netherlands). A printing design of a cuboid with a dimension of 70 × 80 × 1.8 mm (l × w × h) was used for printing. Layer height for the printed structure was set as 0.6 mm and the infill pattern was set as 'aligned rectilinear'. The cuboid-shaped structure was made with three printing speeds (10, 25, and 50 mm/s) using both a straight nozzle (25.4 mm in length) and a tapered nozzle (31.2 mm in length). All experiments were performed at room temperature.

The SC/SA blends were extruded inside a fluid agar gel printing bath. Printed samples were kept at ambient temperature overnight to allow crosslinking of alginate with calcium ions. The printed samples were steamed for 10 min while still present in the fluid agar gel bath. The heating led to melting of the agar fluid gel facilitating removal of the printed samples. Afterwards, the printed samples were washed using Milli Q water and stored for further analysis.

2.7. Compositional analysis

The protein content of the SC-SA stock solution, SC-rich phase, SA-rich phase, and SC/SA blend were determined using a Nitrogen Analyzer (Rapid N cube, Elementar Analysensysteme GmbH) with a nitrogen-to-protein conversion factor of 6.25. The alginate content was calculated as the difference between the dry matter content and the measured protein content. All measurements were performed in duplicate.

2.8. Microscopic analysis

Scanning electron microscope (SEM) (Phenom™ G2 pure, Phenomworld BV, the Netherlands) was performed for visualizing the microstructures of single filament samples and 3D printed samples. All samples were dried overnight in a 40 °C oven before SEM analysis.

Confocal Scanning Laser Microscope (CSLM) analysis was performed to visualize the location of caseinate in the SA-rich phase, SC-rich phase, SC/SA blend, and single filament samples. Rhodamine B (Sigma R 6626, Sigma Aldrich) was diluted with demi water to a concentration of 0.002 wt% and was used for staining sodium caseinate. Samples were visualized with a Confocal Scanning Laser Microscope type 510 (Zeiss, Oberkochen, Germany) using a 543 nm HeNe laser and a 405 nm Blue/Violet diode laser. The images were analyzed with the software ZEN, the blue edition (Carl Zeiss Microscopy).

2.9. Tensile analysis

The mechanical properties of single filaments and 3D printed

samples were measured using a texture analyzer (Stable Micro System, Godalming, UK). The diameters of filaments were measured before the tensile test using a calliper. Young's moduli of samples were obtained via an uniaxial tensile test, which was performed at room temperature with a constant deformation speed of 2.5 mm/s.

Rectangular pieces were cut from 3D printed samples in a shape of 5 × 30 mm both in parallel and perpendicular to the filaments aligning direction. The thickness of the cut rectangular pieces was measured using a digital calliper (Mitutoyo, Kawasaki, Japan) to calculate the initial cross-sectional area. The edges of the cut rectangular pieces were fixed into tensile grips, resulting in an initial length of 24 mm for the sample. The Young's modulus was calculated as the slope of the initial stress-strain curve in the tensile strain range from 0.2 to 0.5. Measurements were done in triplicate.

2.10. Data analysis

Statistical data analysis was done using IBM SPSS statistics (version 25.0). Significant differences among samples were determined using two-way ANOVA followed by Tukey post-hoc tests. A significance level of $p < 0.05$ was chosen for all data analysis. Means together with standard deviation are reported unless stated otherwise.

3. Results and discussion

3.1. Microstructure and composition of SC/SA blend

When sodium caseinate and alginate are mixed in water, aqueous phase separated blends are obtained, creating so called "water in water emulsions" (Capron et al., 2001; Pacek, Ding, Nienow, & Wedd, 2000). The two aqueous phases were separated via centrifugation and recombined to obtain defined SC/SA blends comprising an SC and SA-rich phase. Fig. 3 shows microscopic images of the SA-rich phase and SC-rich phase after centrifugation and the SC/SA blend after recombination. Both the SA-rich phase (Fig. 3a) and the SC/SA blend (Fig. 3c) consist of dispersed caseinate droplets, while the SC-rich phase (Fig. 3b) consists of dispersed alginate droplets. Since the SC/SA blend is a combination of the SC-rich phase and the SA-rich phase from the SC-SA stock solution at a 3:7 ratio, larger caseinate droplets can be expected in SC/SA blends (Fig. 3c) compared to the SA-rich phase (Fig. 3a).

Table 1 shows the composition of the original SC-SA stock solution, SC-rich phase, SA-rich phase, and recombined SC/SA blend. The difference in composition between our blends (Table 1) compared to the blends described previously by Capron et al. (2001) was likely due to the use of ingredients provided by different suppliers and the application of different methods to quantify composition.

Table 1
Compositions of the SC-SA stock solution, SC-rich phase, SA-rich phase, and SC/SA blend.

Composition (wt%)	SC-SA stock solution	SC-rich phase	SA-rich phase	SC/SA blend
Sodium Caseinate content	7.04 ± 0.01	10.08 ± 0.02	1.03 ± 0.01	3.63 ± 0.00
Sodium Alginate content	1.33 ± 0.01	1.11 ± 0.02	2.20 ± 0.01	1.79 ± 0.00

3.2. Extrusion of single filaments

3.2.1. Young's modulus of single printed filaments

To investigate shear-induced structures of SC/SA blends during the 3D printing process, we first extruded the SC/SA blends into a 0.12 wt% calcium chloride solution. Fig. 4 shows Young's moduli of single filaments prepared at different extrusion speeds and using different nozzle types. In general, it was observed that Young's moduli of single filaments decreased with increasing extrusion speed.

For the filaments prepared using straight nozzles, nozzle length did not have significant effect on the Young's modulus ($F_{(2, 27)} = 2.065$, $p = 0.146$), while extrusion speed had a significant effect on the Young's modulus ($F_{(2, 27)} = 17.397$, $p < 0.001$). The Young's moduli of filaments extruded at low speed (10 mm/s) were significantly higher than those extruded at medium speed (25 mm/s) ($p = 0.003$) and at high speed (50 mm/s) ($p < 0.001$). No significant difference was found between filaments extruded at medium (25 mm/s) and high speed (50 mm/s) ($p = 0.094$). There was no significant interaction between the effects of nozzle length and extrusion speed on Young's modulus ($F_{(4, 27)} = 0.98$, $p = 0.435$). From the results one may conclude that fibre strength is not affected by the residence time but more by the velocity profile inside the nozzle affecting the alignment of the emulsion droplets in a different way.

A comparison of the filaments prepared using a tapered nozzle and middle straight nozzle revealed that nozzle type did not have a significant effect on Young's modulus ($F_{(1, 18)} = 0.074$, $p = 0.788$), while extrusion speed had a significant effect on Young's modulus ($F_{(2, 18)} = 16.170$, $p < 0.001$). Young's moduli of filaments extruded at high speed (50 mm/s) were also here significantly lower than those extruded at low speed (10 mm/s) ($p < 0.001$) and those extruded at medium speed (25 mm/s) ($p = 0.008$). No significant difference was found between filaments extruded at low speed (10 mm/s) and those extruded at medium speed (25 mm/s) ($p = 0.095$).

3.2.2. Microstructure of single extruded filaments

Fig. 5 shows SEM images of the surface structures of prepared single filaments. All prepared single filaments appeared to have a micron-sized fibrous structure. As can be observed from Fig. 5, morphologies of filaments extruded with the tapered nozzle were finer than those of
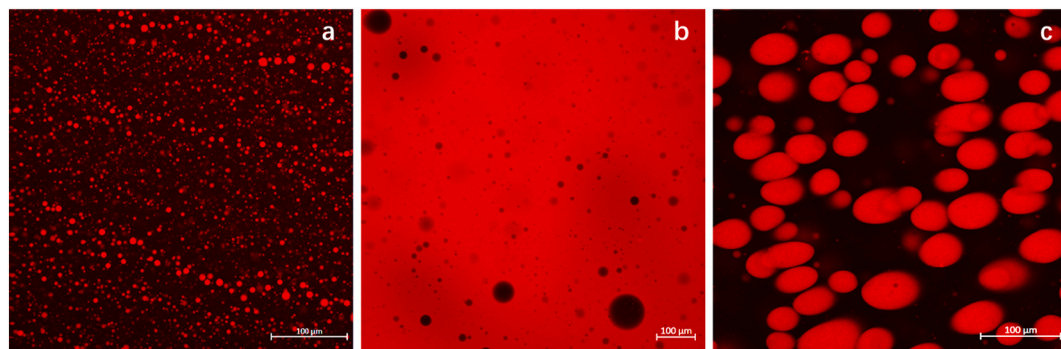

Fig. 3. CSLM images of (a) SA-rich phase, (b) SC-rich phase, and (c) the obtained SC/SA blend. Caseinate is stained in red. (For interpretation of the references to colour in this figure legend, the reader is referred to the web version of this article.)
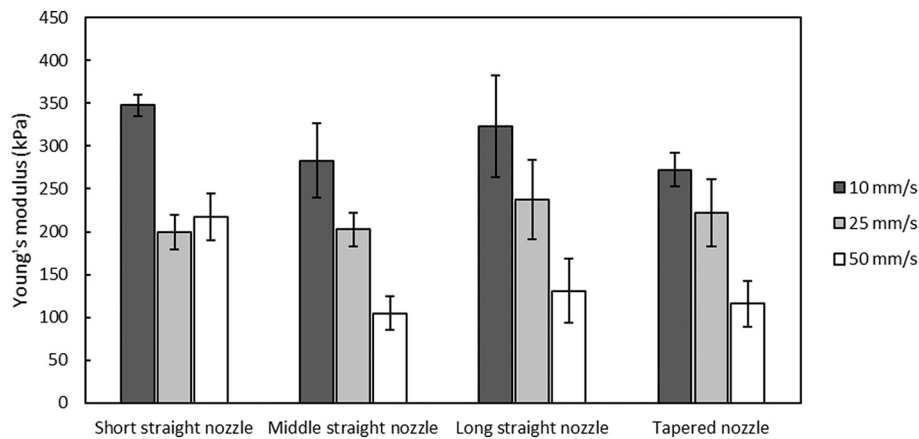
Fig. 4. Young's moduli of single filaments prepared at different extrusion speeds (corresponding to realistic printing speeds) with different nozzle types in a 0.12 wt% CaCl$_2$ solution. Means are shown together with standard deviations.
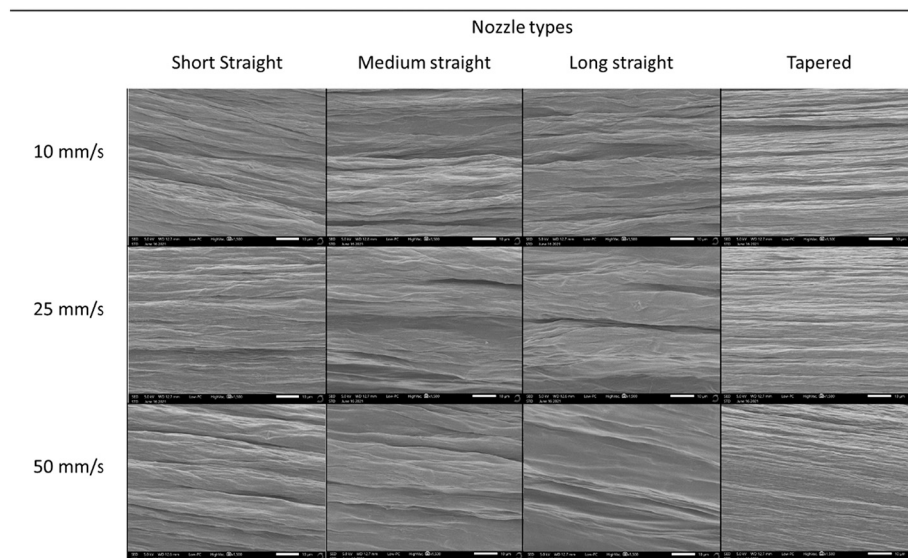

Fig. 5. SEM images of single filaments prepared at different extrusion speeds (corresponding to realistic printing speeds) and with different nozzle types. SEM images were taken at 1500×. Scale bars in the picture correspond to 10 μm.

filaments extruded with straight nozzles. This difference is possibly due to the different radial velocity profiles when extruding with either straight or tapered nozzles. In straight nozzles the velocity profile remains stable along the entire flow direction, whereas in tapered nozzles the velocity gradually increases until the SC/SA blend reaches the nozzle outlet (Reina-Romo et al., 2021). Moreover, during extrusion through straight nozzles we have simple shear flow (laminar flow), while in tapered nozzles also elongational flow is expected. Since elongational flow is more effective to extend droplets than shear flow (Coussot, 2014), caseinate droplets present inside SC/SA blends may be more prone to break up into smaller droplets when extruded using a tapered nozzle. During the extrusion process, the small droplets were stretched into elongated shape in the principal flow direction (Arrigo, Malucelli, & La Mantia, 2021; Coussot, 2014).

Another explanation for the "thicker" fibres observed in filaments extruded from straight nozzles is the formation of several "bands" that were stacked in the vorticity direction. During laminar flow in a straight nozzle, the SC/SA blend moves faster near the centre of the nozzle and remains stationary next to the wall, resulting in a strong velocity gradient perpendicular to the flow direction. Though the exact mechanism is not well understood, various studies have reported the so-called 'vorticity banding' phenomenon in emulsions (Caserta, Simeone, &

Guido, 2008; de Vita, Rosti, Caserta, & Brandt, 2020; Dhont & Briels, 2008). In this study, bands of clustered deformed droplets inside extruded filaments were observed using CSLM (Fig. 6b).

Fig. 6 shows CLSM images of a single filament extruded using a straight nozzle scanned in different depths. The structure of printed filaments consists of elongated caseinate droplets (red) trapped inside crosslinked alginate gel. The elongated caseinate droplets near the filament surface were smaller (Fig. 6a-c) compared to those close to the center of the extruded filament (Fig. 6d-f). It is possible that small caseinate droplets were also elongated close to the center of the extruded filament during extrusion process, but they slowly coalesced into bigger droplets within the time of diffusion of calcium ions used for crosslinking surrounding alginate phase.

3.3. 3D printing in a fluid gel supporting bath

In the current study, we used an agar fluid gel bath to 3D print SC/SA blends. Successful printing was achieved by depositing extruded SC/SA blends and allowing in situ solidification of printed filaments through crosslinking via calcium ions in the agar fluid gel bath.
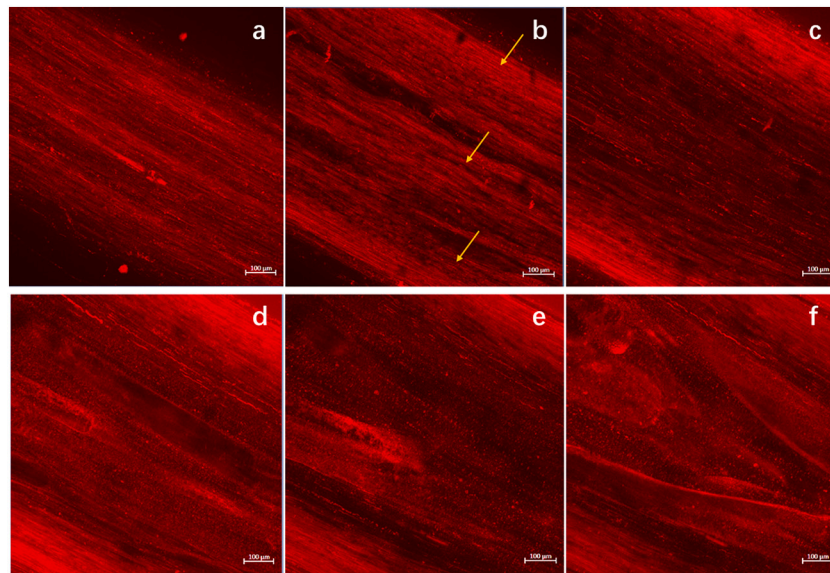
Fig. 6. CLSM images of a single filament extruded using a straight nozzle. Structures were scanned in depths of 20 μm (a), 90 μm (b), 150 μm (c), 220 μm (d), 260 μm (e) and 300 μm (f) from surface to the inner part of a filament. Red colour indicates SC-rich phase. Arraows in Fig. 6b indicate three bands of clustered deformed droplets. (For interpretation of the references to colour in this figure legend, the reader is referred to the web version of this article.)

3.3.1. Influence of CaCl₂ addition procedure on agar fluid gel rheology

The rheological properties of agar fluid gels were largely influenced by the procedure of $CaCl_2$ addition. The influence of $CaCl_2$ addition, either added before the shear-cooling process or mixed afterwards into the prepared agar fluid gel, on storage modulus and recovery behaviour of the agar fluid gel can be found in the Appendix (Fig. A.1). Agar fluid gels with $CaCl_2$ addition before the shear-cooling process had a lower G' and less recovery compared to those with $CaCl_2$ directly mixed into already obtained fluid gels. According to Yu et al. (2020), the addition of ions like calcium reduces the viscosity of agar solutions. If we assume the shear rate to be constant during the shearing-cooling process, the shear stress being proportional to the viscosity of agar solution is likely to decrease with the presence of calcium ions. The reduced shear stress experienced by the growing nuclei may influence the morphology of the final agar gel particles, and both particle size and shape have been reported to have an impact on the rheological behaviour of the agar fluid gel (Ghebremedhin, Seiffert, & Vilgis, 2021; Norton, Jarvis, & Foster, 1999).

Higher G' and recovery percentage of agar fluid gel supporting bath appeared to ensure better entrapment of printed filaments. Fig. 7 shows the printed structures in different agar gel supporting baths. When printing was performed using a fluid agar gel bath with addition of $CaCl_2$ before the shear-cooling process, printed SC/SA filaments were not able to stay in place and were dragged backward when the printing head changed its moving direction (Fig. 7a). Better results were obtained when using a fluid agar gel bath that had $CaCl_2$ addition after fluid gel production (Fig. 7b). Therefore, a supporting bath of fluid agar gel with afterwards added $CaCl_2$ is preferred for 3D printing experiments.

3.3.2. Influence of CaCl₂ concentration on the texture of printed structures

To determine the suitable $CaCl_2$ concentration in the agar fluid gel bath, the Young's moduli of 3D printed structures were measured parallel and perpendicular to the filament orientation. The results are shown in Fig. 8. It can be observed that the Young's moduli measured in parallel direction were higher than those measured in a perpendicular direction. In the parallel direction, the Young's moduli of printed structures increased with increasing $CaCl_2$ content in agar fluid gel bath. The increased Young's modulus may be due to an increased crosslinking density (Li, Wu, He, & Huang, 2016) related to the higher $CaCl_2$ content.

In the perpendicular direction, the Young's moduli of printed structures increased with increasing $CaCl_2$ content up to 0.3%. It was impossible to measure the Young's modulus of the structures printed in the fluid gel bath containing 0.55% $CaCl_2$ since the printed structures easily broke apart in the perpendicular direction when handling. A possible explanation is that at this high $CaCl_2$ concentration crosslinking of the surface of extruded filaments is very fast and thus fusion with neighbouring filaments is prevented. Based on the tensile test results shown in Fig. 8, the agar fluid gel containing 0.25% $CaCl_2$ was chosen
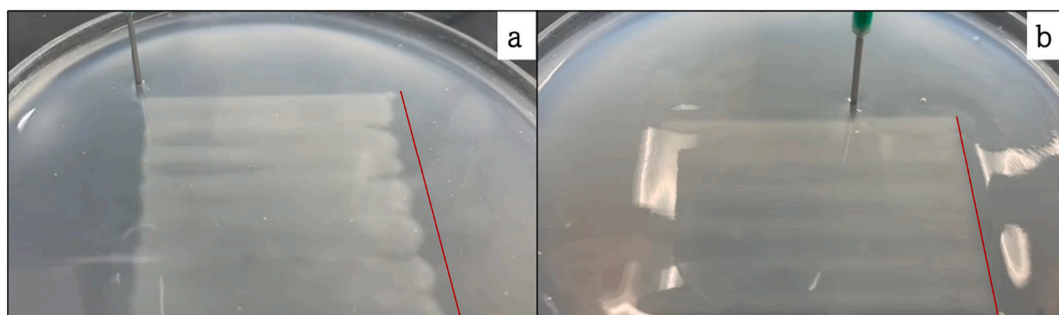

Fig. 7. 3D printing of SC/SA blend in agar fluid gel supporting baths containing 0.25 wt% $CaCl_2$. $CaCl_2$ was either added to hot agar solution before the shear-cooling process (a), or added afterwards to obtained agar fluid gel (b). Red lines indicate the edges of designed printing figures. (For interpretation of the references to colour in this figure legend, the reader is referred to the web version of this article.)
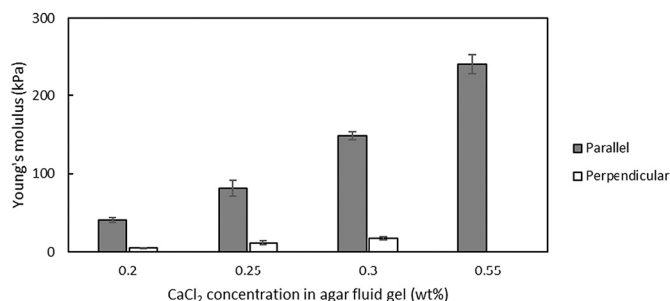
Fig. 8. Young's moduli of 3D printed structures measured in both parallel and perpendicular directions with respect to the filament orientation. 3D printing was performed using a straight medium nozzle with a printing speed of 25 mm/s.

for later study.

3.3.3. 3D printed structures with various shearing profile

The printed structures reduced in size after crosslinking and steaming. A higher degree of size reduction was found in the parallel direction than in the perpendicular direction for all printed samples. The higher degree of size reduction in the parallel direction was probably due to relaxation of the SC/SA blend. The study of Ko et al. (2021) observed the same phenomenon when they post-processed (by oven heating) printed meat analogues that consisted of soy protein paste, sodium alginate and other hydrocolloids. Interestingly, we also observed more size reduction in samples printed with the straight medium nozzle than for the ones printed with the tapered nozzle in both parallel and perpendicular directions.

Fig. 9 shows the Young's moduli of 3D printed samples with either the straight medium nozzle or tapered nozzle at different printing speeds. For samples printed with straight nozzles, the Young's moduli in the parallel direction were much larger than those measured in the perpendicular direction. Differences in Young's moduli in the two directions were less pronounced for samples printed with the tapered nozzle.

In the parallel direction, the nozzle type significantly influenced the Young's modulus (F $(1,12)$ = 18.968, p = 0.001). It is worth mentioning that although the nozzle type did not seem to influence the Young's moduli of filaments that were extruded into $CaCl_2$ solutions (Fig. 4), nozzle type significantly influenced the Young's moduli of 3D printed structures. A possible explanation for this is that the number of filaments in the printed structures subjected to tensile test were different depending on the nozzle type used for printing. As mentioned above, more shrinkage was found in samples printed using the medium straight nozzle than in samples made with the tapered nozzle in a perpendicular direction. The larger size reduction in structures printed with the

straight nozzle resulted thus in a higher fibre density for the defined sample width used in the tensile test. Therefore, although the nozzle type did not influence the Young's moduli of individual filaments (Fig. 4), higher Young's moduli were found for structures 3D printed using straight nozzles (Fig. 9). Printing speed also appeared to have a significant influence on Young's modulus (F $(2,12)$ = 4.582, p = 0.033), where those of the samples printed at 50 mm/s were significantly smaller than those printed at 25 mm/s (p = 0.029).

In perpendicular direction, the nozzle type significantly influenced the Young's modulus (F $(1, 12)$ = 76,335, p < 0.001). This may be due to a better fusion between neighbouring filaments when printing was done using the tapered nozzle as could be derived from SEM pictures Appendix (Fig. A.2). The better fusion suggests less complete crosslinking of alginate at the surface of individual filaments that were extruded using the tapered nozzle allowing subsequent fusion of filaments.

3.4. Potential of 3D printing for making meat-like structures

The 3D printing of SC/SA blends appeared promising to make aligned structures that might be further explored to prepare meat-analogues (Ramachandraiah, 2021). Fig. 10 shows some examples of 3D printed SC/SA anisotropic structures. The appearance of 3D printed SC/SA blends, depending on the calcium content applied for crosslinking, ranged from transparent (gels printed in fluid gel containing 0.12% $CaCl_2$) to turbid and white (gels printed in fluid gel containing 0.3% and 0.55% $CaCl_2$). The appearance might be easily tuned using colouring agents. Individual filaments can be distinguished in 3D printed samples, and the higher the calcium content applied for crosslinking the easier the individual filaments can be visually observed.

The protein content of 3D printed SC/SA blends in this study was around 3.6%, which is lower than that of meat (usually about 20%). A higher protein concentration may be achieved when printing with SC/SA mixtures with a higher caseinate content or using other protein-polysaccharide combinations.

Structures of 3D printed SC/SA blends had both microscale and macroscale fibre alignment which in principle resembles the structure of animal muscle tissue. Texture analysis also indicated that the gel strength was higher in the parallel direction than the perpendicular direction of filament orientation. According to James and Yang (2011), the Young's moduli of a steak (both raw and cooked) is between 70 and 260 kPa. Although the Young's moduli of the printed structures are at the lower end of this range, it should not be too difficult to increase the Young's moduli of 3D printed SC/SA blends further by e.g. adjusting blend composition, printing nozzle type, printing speed, and concentration of calcium ions. Another challenge is to translate those results to plant proteins like those from soy or pea.
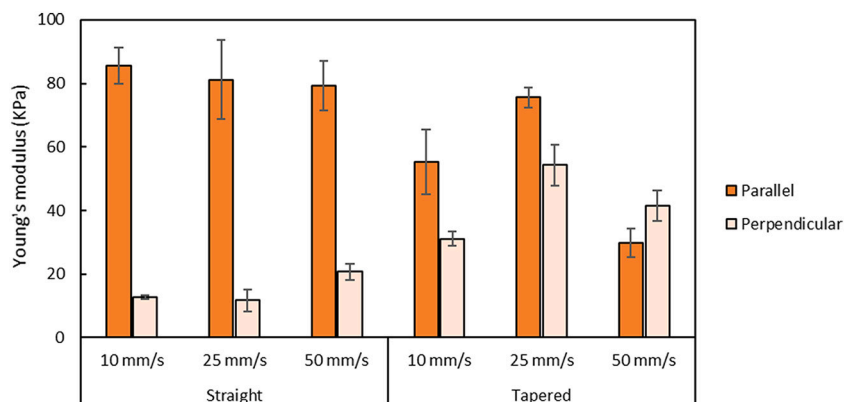

Fig. 9. Young's moduli of samples 3D printed using different printing speeds and nozzle types. Means are shown with standard deviations.
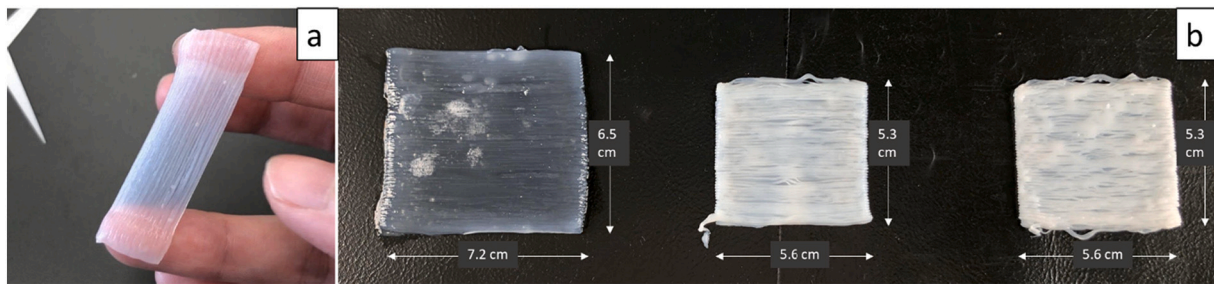
Fig. 10. Examples of 3D printed SC/SA blend samples. (a) a single layer of a 3D printed sample (b) 3D printed structures prepared in agar fluid gel bath containing different CaCl$_2$ content (from left to right: 0.12, 0.3, and 0.55 wt%).

4. Conclusions

This study investigated the influence of shearing profiles on microstructure change of SC/SA blends during the extrusion process and the feasibility of creating both macroscale and microscale aligned fibrous structures using extrusion-based 3D printing technology. We successfully created aligned micron-size fibrous structures and macroscale aligned filament bundles using SC/SA blends. Morphology of extruded filaments differed when using different types of nozzles, and Young's moduli of extruded filaments were significantly influenced by extrusion speed. Calcium-containing agar fluid gel was used as a supporting bath during the 3D printing process, allowing precise deposition and solidification of extruded SC/SA blends. The rheological properties of calcium-containing fluid gels were influenced by the procedure of CaCl$_2$ addition. The addition of CaCl$_2$ directly to agar fluid gels led to a higher storage modulus and recovery percentage. Both nozzle types and extrusion speed were found to influence Young's moduli of 3D printed samples. Compared to the structures printed using a straight nozzle, better fusion among neighbouring filaments was observed in structures printed with a tapered nozzle. This study shows the possibility to create multiscale anisotropic structures using a phase-separated system (e.g. SC/SA blend) by extrusion-based 3D printing technology and might become relevant when striving for products such as meat analogues.

CRediT authorship contribution statement

Sicong Zhu: Conceptualization, Methodology, Investigation, Formal analysis, Writing – original draft. **Wenwei Wang:** Investigation. **Markus Stieger:** Supervision, Writing – review & editing. **Atze Jan van der Goot:** Supervision, Writing – review & editing. **Maarten A.I. Schutyser:** Supervision, Writing – review & editing, Funding acquisition.

Declaration of Competing Interest

None.

Data availability

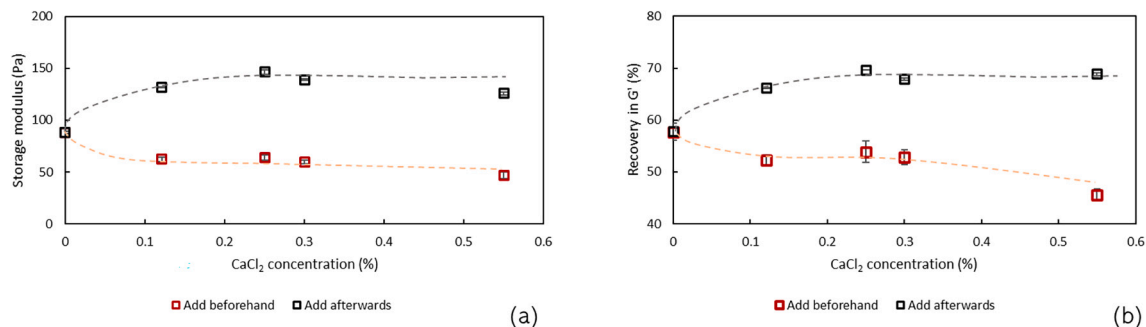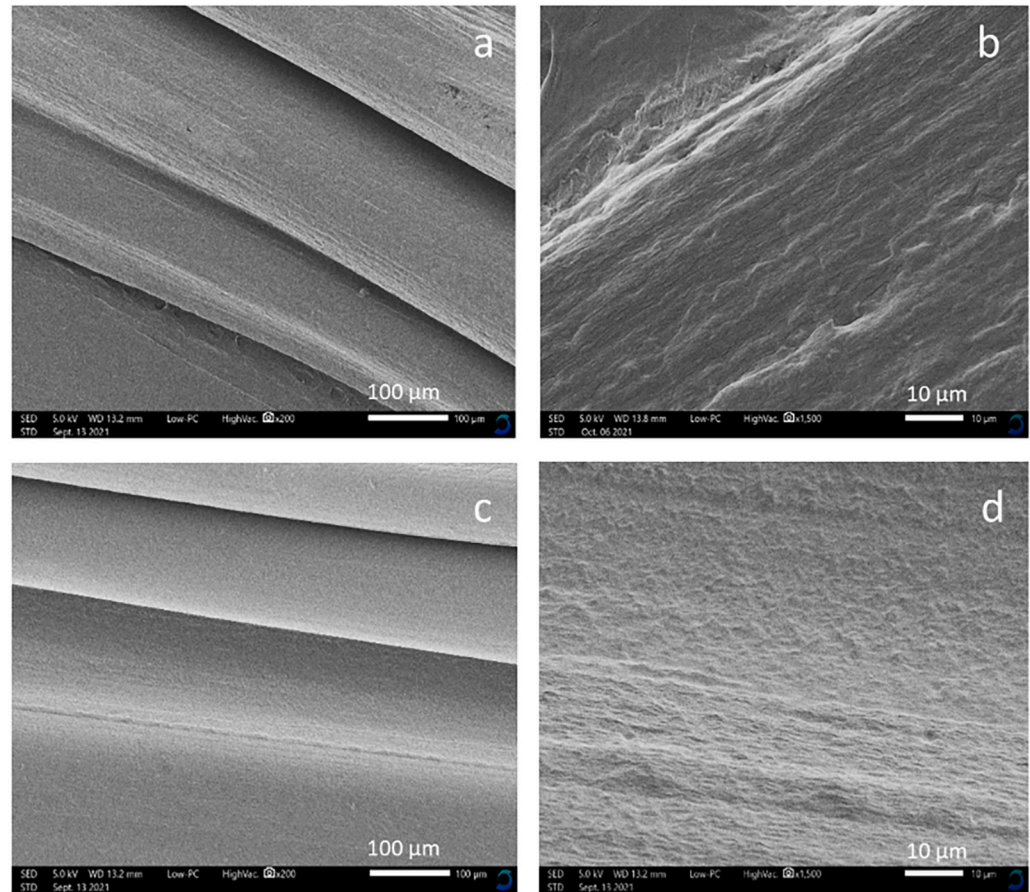Data will be made available on request.

Appendix A. Appendix

Fig. A.1. Storage modulus G' (a) and recovery percentage (b) of agar fluid gel prepared with different CaCl$_2$ addition procedures, either CaCl$_2$ was added before the shear-cooling process (red) or mixed afterwards into the obtained agar fluid gel (black). The recovery percentage is derived from the ratio of G' at 60 s in the third interval compared to the G' value at the end of the first interval. Means are shown with standard deviations. Data points were shown with dashed line as a guide to the eye. (For interpretation of the references to colour in this figure legend, the reader is referred to the web version of this article.)

Fig. A.2. SEM images of 3D printed objects using a medium straight nozzle (a, b) and a tapered nozzle (c, d) at a printing speed of 10 mm/s. SEM images were taken at either 200× (a, c) or 1500× (b, d).

References

Arrigo, R., Malucelli, G., & La Mantia, F. P. (2021). Effect of the elongational flow on the morphology and properties of polymer systems: A brief review. *In Polymers, 13*(20), MDPI. https://doi.org/10.3390/polym13203529

BluRhapsody. (2022). https://blurhapsody.com/en/product/3d-printed-pasta-shapes/.

Capron, I., Costeux, S., & Djabourov, M. (2001). Water in water emulsions: Phase separation and rheology of biopolymer solutions. *Rheologica Acta, 40*(5), 441–456. https://doi.org/10.1007/s003970100161

Caserta, S., Simeone, M., & Guido, S. (2008). Shear banding in biphasic liquid-liquid systems. *Physical Review Letters, 100*(13), 1–4. https://doi.org/10.1103/PhysRevLett.100.137801

Coussot, P. (2014). *Rheophysics - matter in all its states.* https://doi.org/10.1007/978-3-319-06148-1

Dekkers, B. L., Boom, R. M., & van der Goot, A. J. (2018). Structuring processes for meat analogues. In *, Vol. 81. In trends in food science and technology* (pp. 25–36). Elsevier Ltd.. https://doi.org/10.1016/j.tifs.2018.08.011

Dekkers, B. L., Nikiforidis, C.v., & van der Goot, A. J. (2016). Shear-induced fibrous structure formation from a pectin/SPI blend. *Innovative Food Science and Emerging Technologies, 36,* 193–200. https://doi.org/10.1016/j.ifset.2016.07.003

Dhont, J. K. G., & Briels, W. J. (2008). Gradient and vorticity banding. *In Rheologica Acta, 47*(3), 257–281. https://doi.org/10.1007/s00397-007-0245-0

Escalante-Aburto, A., Trujillo-de Santiago, G., Álvarez, M. M., & Chuck-Hernández, C. (2021). Advances and prospective applications of 3D food printing for health improvement and personalized nutrition. *Comprehensive Reviews in Food Science and Food Safety, 20*(6), 5722–5741. https://doi.org/10.1111/1541-4337.12849

Feher, J. (2017). Contractile mechanisms in skeletal muscle. In *Quantitative human physiology* (pp. 305–317). Elsevier. https://doi.org/10.1016/b978-0-12-800883-6.00028-8.

Garrec, D. A., & Norton, I. T. (2012). Understanding fluid gel formation and properties. *Journal of Food Engineering, 112*(3), 175–182. https://doi.org/10.1016/j.jfoodeng.2012.04.001

Ghebremedhin, M., Seiffert, S., & Vilgis, T. A. (2021). Physics of agarose fluid gels: Rheological properties and microstructure. *Current Research in Food Science, 4,* 436–448. https://doi.org/10.1016/j.crfs.2021.06.003

Hinton, T. J., Jallerat, Q., Palchesko, R. N., Park, J. H., Grodzicki, M. S., Shue, H. J., … Feinberg, A. W. (2015). Three-dimensional printing of complex biological structures by freeform reversible embedding of suspended hydrogels. *Science. Advances, 1*(9). https://doi.org/10.1126/sciadv.1500758

Ismail, I., Hwang, Y. H., & Joo, S. T. (2020). Meat analog as future food: A review. In *In journal of animal science and technology (Vol. 62, issue 2, pp. 111–120).* Korean Society of Animal Sciences and Technology. https://doi.org/10.5187/jast.2020.62.2.111.

James, B., & Yang, S. W. (2011). Testing meat tenderness using an in situ straining stage with variable pressure scanning electron microscopy. *Procedia Food Science, 1,* 258–266. https://doi.org/10.1016/j.profoo.2011.09.041

Khemacheevakul, K., Wolodko, J., Nguyen, H., & Wismer, W. (2021). Temporal sensory perceptions of sugar-reduced 3D printed chocolates. *Foods, 10*(9). https://doi.org/10.3390/foods10092082

Kim, S. M., Kim, H. W., & Park, H. J. (2021). Preparation and characterization of surimi-based imitation crab meat using coaxial extrusion three-dimensional food printing. *Innovative Food Science and Emerging Technologies, 71.* https://doi.org/10.1016/j.ifset.2021.102711

Kistler, T., Pridal, A., Bourcet, C., & Denkel, C. (2021). Modulation of sweetness perception in confectionary applications. *Food Quality and Preference, 88,* Article 104087. https://doi.org/10.1016/j.foodqual.2020.104087

Ko, H. J., Wen, Y., Choi, J. H., Park, B. R., Kim, H. W., & Park, H. J. (2021). Meat analog production through artificial muscle fiber insertion using coaxial nozzle-assisted three-dimensional food printing. *Food Hydrocolloids, 120.* https://doi.org/10.1016/j.foodhyd.2021.106898

Kyriakopoulou, K., Dekkers, B., & van der Goot, A. J. (2018). Plant-based meat analogues. In *In sustainable meat production and processing* (pp. 103–126). Elsevier. https://doi.org/10.1016/B978-0-12-814874-7.00006-7.

Li, J., Wu, Y., He, J., & Huang, Y. (2016). A new insight to the effect of calcium concentration on gelation process and physical properties of alginate films. *Journal of Materials Science, 51*(12), 5791–5801. https://doi.org/10.1007/s10853-016-9880-0

Norton, I. T., Jarvis, D. A., & Foster, T. J. (1999). A molecular model for the formation and properties of fluid gels. In *International Journal of Biological Macromolecules, 26.* www.elsevier.com/locate/ijbiomac.

Pacek, A. W., Ding, P., Nienow, A. W., & Wedd, M. (2000). Phase separation and drop size distributions in "homogeneous" Na-alginate/Na-caseinate mixtures. *Carbohydrate Polymers, 42*(4), 401–409. https://doi.org/10.1016/S0144-8617(99)00181-2

Pietsch, V. L., Bühler, J. M., Karbstein, H. P., & Emin, M. A. (2019). High moisture extrusion of soy protein concentrate: Influence of thermomechanical treatment on protein-protein interactions and rheological properties. *Journal of Food Engineering, 251*, 11–18. https://doi.org/10.1016/j.jfoodeng.2019.01.001

Ramachandraiah, K. (2021). Potential development of sustainable 3d-printed meat analogues: A review. *In sustainability (Switzerland), 13*(2), 1–20. MDPI https://doi.org/10.3390/su13020938.

Reina-Romo, E., Mandal, S., Amorim, P., Bloemen, V., Ferraris, E., & Geris, L. (2021). Towards the experimentally-informed in silico nozzle design optimization for extrusion-based bioprinting of shear-thinning hydrogels. *Frontiers in Bioengineering and Biotechnology, 9*. https://doi.org/10.3389/fbioe.2021.701778

Schreuders, F. K. G., Sagis, L. M. C., Bodnár, I., Erni, P., Boom, R. M., & van der Goot, A. J. (2021). Small and large oscillatory shear properties of concentrated proteins. *Food Hydrocolloids, 110*. https://doi.org/10.1016/j.foodhyd.2020.106172

Sun, J., Zhou, W., Huang, D., Fuh, J. Y. H., & Hong, G. S. (2015). An overview of 3D printing Technologies for Food Fabrication. *Food and Bioprocess Technology, 8*(8), 1605–1615. https://doi.org/10.1007/s11947-015-1528-6

Takayama, Y., & Kato, N. (2018). Shear-induced structuring for multiple parallel gel filaments obtained from casein-alginate hybrids. *Langmuir, 34*(44), 13352–13360. https://doi.org/10.1021/acs.langmuir.8b03038

Tolstoguzov, V. (2006). Texturising by phase separation. *Biotechnology Advances, 24*(6), 626–628. https://doi.org/10.1016/j.biotechadv.2006.07.001

de Vita, F., Rosti, M. E., Caserta, S., & Brandt, L. (2020). Numerical simulations of vorticity banding of emulsions in shear flows. *Soft Matter, 16*(11), 2854–2863. https://doi.org/10.1039/c9sm01898k

Yu, Z., Zhan, J., Wang, H., Zheng, H., Xie, J., & Wang, X. (2020). Analysis of influencing factors on viscosity of agar solution for capsules. *Journal of Physics: Conference Series, 1653*(1). https://doi.org/10.1088/1742-6596/1653/1/012059

Zhu, S., Vazquez, I., de Azua, R., Feijen, S., Jan, A., der Goot, V., Schutyser, M., & Stieger, M. (2021). How macroscopic structure of 3D printed protein bars filled with chocolate influences instrumental and sensory texture. *LWT, 151*(May), Article 112155. https://doi.org/10.1016/j.lwt.2021.112155